Detection and quantification of lateral, illicit connections and infiltration in sewers with Infra-Red camera

Conclusions after a wide experimental plan

Lepot, Mathieu; Makris, Konstantinos F.; Clemens, François H.L.R.

DOI
10.1016/j.watres.2017.06.030

Publication date
2017

Document Version
Final published version

Published in
Water Research

Citation (APA)
Lepot, M., Makris, K. F., & Clemens, F. H. L. R. (2017). Detection and quantification of lateral, illicit connections and infiltration in sewers with Infra-Red camera: Conclusions after a wide experimental plan. *Water Research*, *122*, 678-691. https://doi.org/10.1016/j.watres.2017.06.030

Water Research 122 (2017) 678–691

Contents lists available at ScienceDirect

Water Research

journal homepage: www.elsevier.com/locate/watres

Detection and quantification of lateral, illicit connections and infiltration in sewers with Infra-Red camera: Conclusions after a wide experimental plan

Mathieu Lepot [a, *], Konstantinos F. Makris [a], François H.L.R. Clemens [a, b]

[a] Water Management Department, Faculty of Civil Engineering and Geosciences, Delft University of Technology, Stevinweg 1 (Building 23), 2628 CN Delft, The Netherlands
[b] Deltares, P.o. Box 177, 2600 MH Delft, The Netherlands

ARTICLE INFO

Article history:
Received 20 December 2016
Received in revised form
28 April 2017
Accepted 11 June 2017
Available online 12 June 2017

Keywords:
Connection
Separate sewer
Identification
Quantification
Thermography

ABSTRACT

Separate sewer systems are sensitive to illegal or mis-connections. Several techniques (including the Distributed Temperature Sensor) are now available to identify and locate those connections. Based on thermal fingerprints, DTS allows the localization of each lateral connection along a reach. The use of Infra-Red camera has been investigated with 748 laboratory experiments (artificial connections along a flume). The tested connections vary in diameters (from 75 to 200 mm), lengths of intrusion (from 0 to 200 m), shapes (circular or linear *i.e.* cracks), depths, discharge rates between the lateral connection and the main flume, and temperatures. IR frame analysis (for detection) and 2D temperature mapping (at the free water surface, for quantification) demonstrate that: *i)* the detection limit is very low (ratio between lateral and main discharges: 0.025) and *ii)* the quantification of the lateral discharge is impossible. Application of an IR camera seems to be a promising technique to detect lateral connections.

1. Introduction

Sewer systems are capital extensive and aging structures. Along their lifetime, *i.e.* from their construction to their replacement, they are liable to cracks and misconnection occurrences. The wastewater of approximately 25% of the households in the Netherlands is discharged into separate sewer systems (Schilperoort et al., 2013). This tendency for using separate systems for the discharge of different types of water could be easily justified by some theoretical advantages that separate systems are expected to offer (reduction of health risks, recycling of run-off water, *reduction of the load on the receiving WWTP and a reduction of uncontrolled discharge of diluted wastewater on receiving water bodies*). However, the major disadvantage that is usually observed is the existence of illicit or misconnections. The combination with the absence of inspection or treatment of storm water results in the direct discharge of raw sewage to the receiving waters. Very commonly used techniques (Panasiuk et al., 2015) for the detection of illicit connections are the smoke test and the dye test (Hoes et al., 2009) and the use of fiber-optic DTS (Nienhuis et al., 2013). While, for most cases, the inspection is usually restricted by the water level within the pipe, the current research strives to give a more comprehensive approach to the detection of illicit connections and groundwater infiltration with the use of thermography.

Several purposes can be reached by the different kind of inspection techniques: *i)* the detection of potential misconnection(s), *ii)* their localisations and *iii)* their quantifications. Those techniques can produce data in time or/and space: the records of time series, as of temperature (Schilperoort et al., 2006) or conductivity (Deffontis et al., 2013), allow the detection and, sometimes, the quantification (e.g. in de Bénédittis and Bertrand-Krajewski, 2005, 2015) of lateral connections or/and infiltrations. However, due to the single place location of the sensor, the localization of the misconnection is not feasible. Other techniques can provide a spatial detection: visual inspections (Butler and Davies, 2004), sometimes combined with the temporal sensitivity such as the DTS (Hoes et al., 2009). Most of the techniques reviewed by Panasiuk et al. (2015) present some drawbacks: DTS requires the installation of the cable in the sewer, dye and smoke testing are time consuming, odour or visual inspection are, by definition, sensitive to human subjectivity while methods based on sample analysis may be costly.

The present study uses an IR camera, as Lega and Napoli (2010)

* Corresponding author.
E-mail address: m.j.lepot@tudelft.nl (M. Lepot).

http://dx.doi.org/10.1016/j.watres.2017.06.030

did, but within the sewer in order to allow a spatial detection of active (leaking) lateral connections. Hence, a lateral connection without any flow cannot be identified by the presented technique. Finally, based on a fundamental thermodynamic balance, a quantification method is proposed and tested on 748 laboratory experiments. Detection and quantification limits are eventually quantified and discussed.

2. Materials and methods

2.1. Experimental set up

Experiments have taken place on the Eastern Scheldt flume in Deltares. The experimental setup was divided in three parts.

The main flume. This rectangular channel is built with glass windows and a steel structure: 1 m width, 1.2 m high and 50 m long (42 m of glass windows + start and end in concrete). Supplied by a pump (Flowserve, MI10), the flow is controlled by the frequency of the supply and measured with an electromagnetic flowmeter (Endress + Hauser, Promag W) of 600 mm diameter. Hydraulic conditions are controlled by a wall valve located downstream, at the end of the flume.

The sensor train. On top of the steel structure, a railway allows the perfectly parallel translation of the moving structure. On this train, an uncooled IR camera (Flir, A35sc) and an accurate distance meter (Dimetix, FLS-C10) have been installed and connected to their respective laptops. Fig. 1 presents the two data acquisition systems. This platform was manually moved during the experiments and its position was recorded by the laser data (see Fig. 2).

The tank and the lateral connections. In order to simulate lateral connections, special windows with several connection types (Table 1) have been mounted on the flume. Lateral connections have been supplied by warm (heated with a pasteuriser - TomPress, Pasteurisateur thermoplongeur à jus) and cold (cooled with crushed ice) water, stored in a 0.91 m^3 tank.

In order to ensure a uniform distribution of the temperature, water has been mixing with a mixer (Shaft length: 650 mm, Shaft diameter: 30 mm, Overall diameter: 170 mm): the rotation frequency has been fixed to 30 Hz. A 10 m pipe (diameter of 50 mm) has been used for the connection between the tank and the special windows. In order to ensure connection with small diameters (Table 1, diffusor and mixed – Di connection), an extra pipe (32 mm, 2 m) has been added (with a 50-32 mm diameter reduction) while needed. Discharges from the tank to the flume have been controlled with a manual quarter valve and calculated via lost volume (difference in water levels, before and after the opening, measured with a ruler) and the opening duration (recorded by a chronometer application).

2.2. Laboratory experiments

Hundreds of experiments have been done during two months. Each lateral connection (Table 1) has been tested with warm and cold water, for each hydraulic condition in the flume (Table 2) and for three valve openings (from the tank to the flume: 100, 50 and 10%).

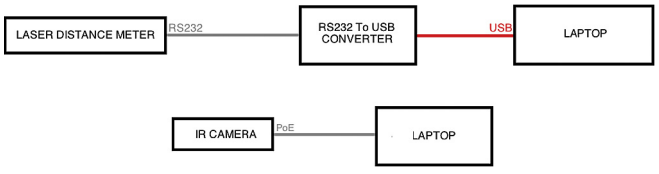

Fig. 1. Schemas of the two data acquisition systems.

Additionally to all the combinations, other experiments have been performed: blank measurement for each hydraulic condition, repeated measurements (by triplicates), measurement with different moving speed of the IR camera, from upstream to downstream measurements. In total, 748 experiments have been done.

2.3. Method

2.3.1. Sensor calibrations

Both the uncooled IR camera and laser distance meter need to be calibrated.

IR camera calibration. IR cameras present vignetting and distortion phenomena due to the transition between the cylindrical lens and the rectangular sensor. Despite the fact that calibration of standard cameras is easy using a checkerboard (refs), the calibration of IR camera presents some additional difficulties. The IR camera has just been calibrated for tangential and radial distortion (Eq. (1)), in three steps. Firstly, a black and white checkerboard has been placed behind a window (sun light) and the black squares became warmer than the white ones. Then, frames have been recorded for 20 different relative positions of the board. Finally, the calibration has been done with the camera calibration tool of Matlab©. Vignetting has not been calibrated for this study.

$$\begin{cases} x_{DISTORED} = x \times \left(1 + k_1 \times r^2 + k_2 \times r^4 + k_3 \times r^6\right) \\ y_{DISTORED} = y \times \left(1 + k_1 \times r^2 + k_2 \times r^4 + k_3 \times r^6\right) \end{cases} \quad (1a)$$

$$\begin{cases} x_{DISTORED} = x + \left[2 \times p_1 \times y + p_2 \times \left(r^2 + 2 \times x^2\right)\right] \\ y_{DISTORED} = y + \left[p_1 \times \left(r^2 + 2 \times y^2\right) y + 2 \times p_2 \times x\right] \end{cases} \quad (1b)$$

where x and y are undistorted pixel locations, $x_{DISTORTED}$ and $y_{DISTORTED}$ are distorted pixel locations, $r^2 = x^2 + y^2$, k_1, k_2 and k_3 are the radial distortion coefficients of the lens and p_1 and p_2 are the tangential ones.

Laser distance meter calibration. This calibration has been done with the method presented by Bertrand-Krajewski (2008) and N_{CD} calibration distances (1, 3, 5, 7, 9, 11, 13, 15, 17, 19, 21, 23, 25, 27, 29, 31 and 33 m). Measured distances have been repeatedly measured (N_M times) for each calibration distance. Based on Williamson (1968), reviewed (Reed, 1989) and corrected (Reed, 1992), the method proposed by Bertrand-Krajewski (2008) aims to numerically minimise the goal function defined by equation (2) where $D_{R,i}$ is a linear or polynomial function (2nd or 3rd order) of $d_{M,i}$.

$$S = \sum_{i=1}^{N_{CD}} \left[\frac{1}{u^2(d_{R,i})} \times \left(D_{R,i} - d_{R,i}\right)^2 + \frac{1}{u^2(d_{M,i})} \sum_{j=1}^{N_M} \left(D_{M,i,j} - d_{M,i,j}\right)^2 \right] \quad (2)$$

where $d_{R,i}$ is the real (*i.e.* calibration) distance of index i (in m) among the N_{CD} (17) ones, $u(d_{R,i})$ is standard uncertainty (in m), $D_{R,i}$ is the one estimated by the calibration model (in m), $d_{M,i,j}$ (in m) is the jth measurement for the distance i and $D_{M,i,j}$ (in m) is the one estimated by the calibration model and $u(d_{M,i})$ is the standard deviation (in m) of the N_M (1200) $d_{M,I,j}$.

2.3.2. Data processing

Data pre-processing. Raw data requires being pre-processed before further analyses and calculations. For the laser distance meter, the measured distances need to be corrected by the inverse

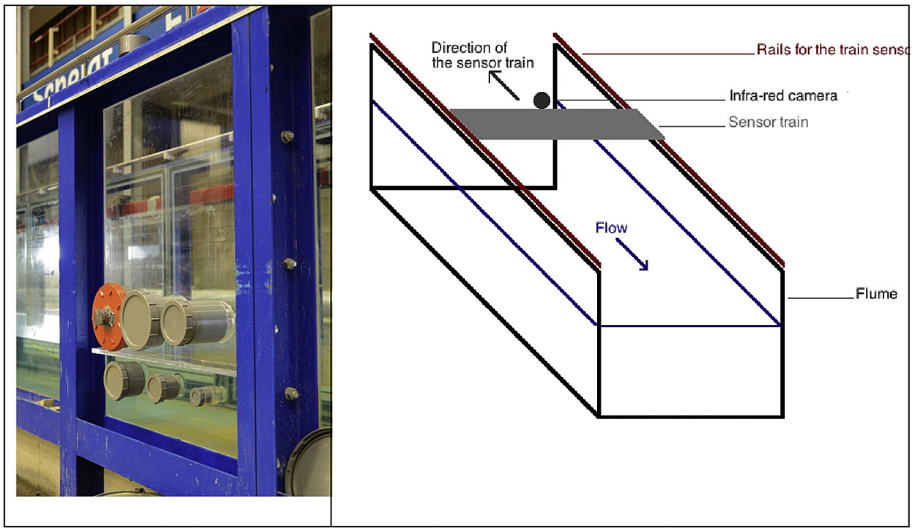

Fig. 2. Left: the experimental setup, photo of the diameter windows set up on the right bank of the Eastern Scheldt flume. Right: Scheme of the sensor train and the flume.

Table 1
List of lateral connections (Sketchup© screenshots are presented in Appendix A).

Windows	Name of connection	Description
Diameters	D 200 mm D 160 mm D 100 mm	Several diameters, located at 400 mm from the invert level (centre of the connection)
Water levels	WL 200 mm WL 400 mm WL 600 mm WL 800 mm WL 1000 mm	100 mm diameter, located at several water level i.e. from invert level (centre of the connection)
Intrusion	I 50 mm I 100 mm I 150 mm I 200 mm	100 mm diameter, located at 200 mm (I 100 and I 200) and 400 mm (I 50 and I 150) from the invert level (centre of the connection)
Diffuser	Di 0 Di 45 Di 90	Line of 5 mm diameter holes (1 every 10 mm)
Mixed	M_Di - 45 M_D 75 mm M_I 50 mm	Mixed condition windows: I 50 is 100 mm diameter (centre located at 400 mm from the invert level)

calibration function from the measured distances. The raw IR camera data requires more effort: vignetting and distortion corrections and the transformation of pixel values to temperatures (Eq. (3)).

$$T = \frac{B}{\ln\left[\frac{R}{(S-O)} + F\right]} - 273.15 \quad (3)$$

where T is the temperature (in °C), B, R, O and F are Planck constants, which derive from the factory thermal calibration of each individual infrared camera, and S is the 14 bits digital signal value.

Data conversion. With the corrected data, two types of end-user data have been created: *i)* grey and blue-red scale videos and *ii)* 2D temperature maps. Initially scaled for the full temperature range (from - 25 C to 135 C), the range has been rescaled from the minimal to the maximal recorded temperatures to increase the image/video readability.

The creation of end-user friendly videos did not require any specific method except for the rescaling.

The creation of the 2D maps requires laser data, the camera position and orientation, and the post-synchronisation of both data acquisition systems. Laser data and IR camera frames have been recorded on two different laptops (Fig. 1), which may have two different clocks: the synchronisation between both clocks is mandatory to allocate the right position (laser data) to the right IR camera frame. After the conversion of pixel value to temperature value (Eq. (3)), each frame has been analysed and positioned according to the following procedure. The correspondence between the horizontal plane of the flume and the acquired frames has been achieved by taking into account the camera's spatial position along the flume (in the middle, at 45° with respect to the longitudinal axes of the flume) and the angular view of the camera (vertical 39° and horizontal 48°, manufacturer data). The design of the maps is based on the translation of the camera's resolution (256 × 320) to a square grid of 1 × 1 mm, followed by the assumption that the water level is steady within the spatial range of measurements. The camera was set to record at 60 frames per second, resulting in

Table 2
List of hydraulic conditions during the experiments.

Code for the experimental conditions	Discharge in the flume - upstream the lateral connection (Q_U) (l/s)	Position of the wall valve (m)	Average velocity at 20 m from the wall valve (m/s)	Reynolds number (without unit) $N_{RE} = u^*R_h/\nu$
1a	100	0.70	0.12	37 500
	100	0.30	0.23	52 500
1b	120	0.30	0.26	62 500
2	200	0.60	0.25	75 000
3	300	0.50	0.38	116 250
4	400	0.40	0.54	160 000
5a	500	0.30	0.71	206 250
5b	520	0.30	0.72	212 500

acquiring temperature values in numerous frames for the same positions in the flume. During the creation of the maps every square in the grid is depicted with the average of these temperature values. The outcome of this method is the improvement of the produced visualisations of the water surface, as the vignetting effect and other external factors that may introduce noise and bias (e.g. the reflection of the ceiling lights) are up to a point reduced.

2.3.3. Detection of lateral connections

The detection of foreign bodies in the flume is based on the thermal differences that exist between consecutive frames in the acquired videos. Through the formed cloud, the possible perturbation due to a lateral connection can be detected with a variance test: if equation (4) is not satisfied, the temperature of the pixel is significantly different from one frame to the next one.

$$|T_i - T_{i-1}| \leq 2 \times (u(T_i) + u(T_{i-1})) \tag{4}$$

where T_i (°C), and T_{i-1} (°C), are the respective temperatures recorded on a pixel during the experiment in two consecutive frames (i and i-1); and where $u(T_i)$ and $u(T_{i-1})$ are their standard uncertainties (°C).

In order to avoid detection of artefacts, a lateral connection has been considered as detectable if there is a difference in the thermal status of at least 9 grouped pixels within the range of 60 consecutive frames (*i.e.* 1 s). These values arose after testing several combinations on experiments that presented intense effects of artefacts (*i.e.* the reflection of the ceiling lights), and were afterwards applied to the whole range of experiments.

2.3.4. Quantification of lateral connections

While considering water masses along the reach (the lateral connection and the pipe: upstream and downstream) and due to the high frequency of the IR camera (60 fps), the system can be considered as adiabatic. Right at the lateral connection, no other external source or well of energy may affect the temperature distribution at the free surface. This is a strong simplifying assumption but the following balance can be written (Eq. (5)):

$$Q_{LC,IR} \times T_{LC} + Q_U \times T_U = Q_D \times T_D \tag{5}$$

where $Q_{LC,IR}$, Q_U and Q_D are the discharges (in l/s) of the lateral connection, the main pipe upstream and downstream of the lateral connection respectively with their respective temperatures (T_{LC}, T_U and T_D in °C).

While assuming no leakage and no other lateral connection, equation (5) can be re-written as following (Eq. (6)).

$$Q_{LC,IR} \times T_{LC} + Q_U \times T_U = (Q_{LC,IR} + Q_U) \times T_D \tag{6}$$

And Q_{LC} is finally calculated (Eq. (7)).

$$Q_{LC,IR} = Q_U \times \frac{T_D - T_U}{T_{LC} - T_D} \tag{7}$$

T_{LC} can be estimated in three different manners: *i)* a direct measurement of the temperature with IR image if the connection is above the water level (water fall), *ii)* estimation of the maximal or minimal values with IR data if the connection is below the water level (the real temperature is equal or colder, and respectively equal or warmer, than the maximal value at the free surface for cold, and respectively warm, lateral connections) and *iii)* estimation by other measurements or estimations (as for temperatures of ground water tables). In case the second manner is applied, the discharge from the lateral connection can be delimited as following (Equation (8), for cold lateral connection and Equation (9) for warm lateral connection):

$$Q_{LC,IR} \geq Q_U \times \frac{T_D - T_U}{T_{LC,EST-COLD} - T_D} \tag{8}$$

$$Q_{LC,IR} \leq Q_U \times \frac{T_D - T_U}{T_{LC,EST-WARM} - T_D} \tag{9}$$

where $T_{LC,EST-COLD}$, and respectively $T_{LC,EST-WARM}$, are the estimated temperatures (°C) of the cold, and respectively warm, lateral connections assuming to be equal to the minimal, and respectively the maximal, temperature of the free surface.

The application of the law of uncertainty propagation (JCGM 104, 2009) to equation (7) leads to the estimation of standard uncertainty of the lateral connection (Eq. (10)).

$$u(Q_{LC,IR}) = \sqrt{\begin{aligned} &u^2(Q_U) \times \left(\frac{T_D - T_U}{T_{LC} - T_D}\right)^2 + u^2(T_U) \times \left(\frac{Q_U}{T_{LC} - T_D}\right)^2 \\ &+u^2(T_D) \times \left(\frac{Q_U \times (T_{LC} - T_U)}{(T_{LC} - T_D)^2}\right)^2 + u^2(T_{LC}) \times \left(\frac{Q_U \times (T_D - T_U)}{T_{LC}^2}\right)^2 \\ &+2 \times cov(T_U, T_D) \times \left(\frac{Q_U}{T_{LC} - T_D}\right) \times \left(\frac{Q_U \times (T_{LC} - T_U)}{(T_{LC} - T_D)^2}\right) \\ &+2 \times cov(T_U, T_{LC}) \times \left(\frac{Q_U}{T_{LC} - T_D}\right) \times \left(\frac{Q_U \times (T_D - T_U)}{T_{LC}^2}\right) \\ &+2 \times cov(T_D, T_{LC}) \times \left(\frac{Q_U \times (T_{LC} - T_U)}{(T_{LC} - T_D)^2}\right) \times \left(\frac{Q_U \times (T_D - T_U)}{T_{LC}^2}\right) \end{aligned}} \tag{10}$$

where $u(Q_U)$ (in l/s) is the standard uncertainty on Q_U, $u(T_U)$ (in K) is the standard uncertainty on T_U, $u(T_{LC})$ (in °C) is the standard uncertainty on T_{LC}, $u(T_D)$ (in °C) is the standard uncertainty on T_D and under the assumption that there is no correlation between the temperatures (T_{LC}, T_U and T_D) and the discharge upstream the lateral connection.

Since T_U and T_D are measured in the same pipe, by the same

camera connected to the same data acquisition system, $cov(T_U,T_D)$ is assumed to be equal to $u(T_U).u(T_D)$. Depending on how T_{LC} is measured or estimated, equation (10) is finally simplified to equation (11a), and equation (11b), when T_{LC} is estimated or measured with IR data, and with another way respectively.

$$u(Q_{LC,IR}) = \sqrt{\begin{array}{c} u^2(Q_U) \times \left(\frac{T_D - T_U}{T_{LC} - T_D}\right)^2 + u^2(T_U) \times \left(\frac{Q_U}{T_{LC} - T_D}\right)^2 \\ +u^2(T_D) \times \left(\frac{Q_U \times (T_{LC} - T_U)}{(T_{LC} - T_D)^2}\right)^2 + u^2(T_{LC}) \times \left(\frac{Q_U \times (T_D - T_U)}{T_{LC}^2}\right)^2 \\ +2 \times u(T_U) \times u(T_D) \times \left(\frac{Q_U}{T_{LC} - T_D}\right) \times \left(\frac{Q_U \times (T_{LC} - T_U)}{(T_{LC} - T_D)^2}\right) \\ +2 \times u(T_U) \times u(T_{LC}) \times \left(\frac{Q_U}{T_{LC} - T_D}\right) \times \left(\frac{Q_U \times (T_D - T_U)}{T_{LC}^2}\right) \\ +2 \times u(T_D) \times u(T_{LC}) \times \left(\frac{Q_U \times (T_{LC} - T_U)}{(T_{LC} - T_D)^2}\right) \times \left(\frac{Q_U \times (T_D - T_U)}{T_{LC}^2}\right) \end{array}} \quad (11a)$$

$$u(Q_{LC,IR}) = \sqrt{\begin{array}{c} u^2(Q_U) \times \left(\frac{T_D - T_U}{T_{LC} - T_D}\right)^2 + u^2(T_U) \times \left(\frac{Q_U}{T_{LC} - T_D}\right)^2 \\ +u^2(T_D) \times \left(\frac{Q_U \times (T_{LC} - T_U)}{(T_{LC} - T_D)^2}\right)^2 + u^2(T_{LC}) \times \left(\frac{Q_U \times (T_D - T_U)}{(T_{LC} - T_D)^2}\right)^2 \\ +2 \times u(T_U) \times u(T_D) \times \left(\frac{Q_U}{T_{LC} - T_D}\right) \times \left(\frac{Q_U \times (T_{LC} - T_U)}{(T_{LC} - T_D)^2}\right) \end{array}} \quad (11b)$$

The discharge coming from the lateral connection and calculated with equation (7) is finally compared to the known discharge ($Q_{LC,TRUE}$ in l/s) calculated with the difference on the water levels in the tank and the duration (d in s) of the opening of the valve (Eq. (12a)) and its standard uncertainty (Eq. (12b)), estimated according to

$$Q_{LC,TRUE} = \frac{A_{TANK} \times (h_{BEGINNING} - h_{END})}{d} \quad (12a)$$

$$u(Q_{LC,TRUE}) = \sqrt{\begin{array}{c} u^2(A_{TANK}) \times \left[\frac{(h_{BEGINNING} - h_{END})}{d}\right]^2 \\ +\left(\frac{A_{TANK}}{d}\right)^2 \times (u(h_{BEGINNING}) - u(h_{END}))^2 \\ +u^2(d) \times A_{TANK}^2 \times \left[\frac{h_{BEGINNING} - h_{END}}{d^2}\right]^2 \end{array}} \quad (12b)$$

where $h_{BEGINNING}$ and respectively h_{END} are the water levels (in m) in the tank (of an area A_{TANK} in m^2) before and respectively after the opening of the valve. Due to the fact that $Q_{LC,IR}$ and $Q_{LC,TRUE}$ are estimated by two completely independent methods, the lateral connection is considered as quantifiable if equation (13) is satisfied (variance test).

$$|Q_{LC} - Q_{LC,TRUE}| \leq 2 \times \sqrt{u^2(Q_{LC}) + u^2(Q_{LC,TRUE})} \quad (13)$$

3. Results and discussion

3.1. Sensor calibrations

The laser distance meter offers a good linearity: the straight-line function has been retained (Fig. 3) by a Fischer-Snedector test.

Table 3 summarises the distortion coefficients for the IR camera (Eq. (1)).

Fig. 4 illustrates the distortion correction done for each frame. By comparison to the left image (raw), the intersections between the flume and the free surface clearly appears as straight lines on the right image (corrected).

3.2. Detection and quantification limits of the proposed methods

Based on the experiments and the methods previously described, experiments present three possible results. The lateral connection is *i)* not detectable, *ii)* detectable but not quantifiable,

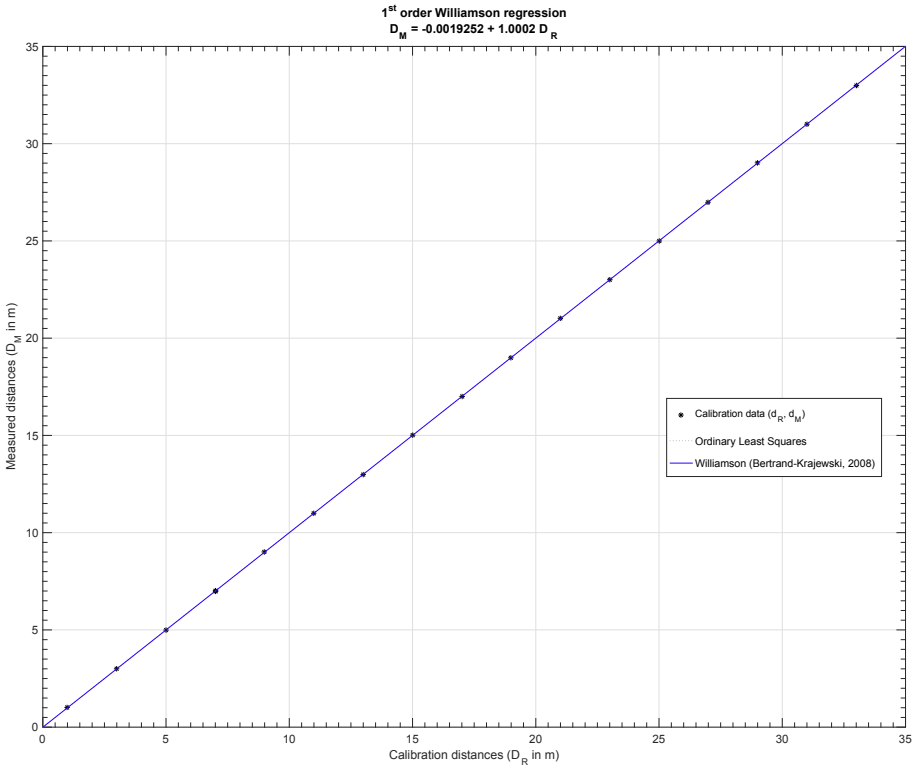

Fig. 3. 1st order polynomial for the calibration of the laser distance meter.

Table 3
Distortion coefficient of the IR camera.

Radial Coefficients			Tangential Coefficients	
k_1	k_2	k_3	p_1	p_2
0.438	0.143	0.171	$-5.228\ 10^{-4}$	0.002

iii) detectable and quantifiable.

3.2.1. Lateral connection detection

Fig. 5 shows the rescaling effect and highlights the need of end-user adapted temperature scale. The non-rescaled one (left) appears to be neutral grey: the range of temperatures measured during the experiments is very narrow by comparison to the measuring range of the IR camera.

This first treatment allows a manual detection (or validation) of the presence of a lateral connection. Fig. 6 shows the variance test applied between two consecutive frames: the pixels that don't satisfy Eq. (4) are plotted in white on the right figure.

The lateral connection is clearly visible on the blue-red scaled frames. The proposed algorithm is as well able to detect significant difference in the thermal fingerprint (groups of white pixel on the right picture).

Among the 748 experiments, 732 present the record of active lateral connections (485 pipes and 263 diffusors). All connections above the free surface are obviously detectable.

The detection limit ($Q_{LC,TRUE}/Q_U$) is sensitive to the relative depth of the connection with respect to the water level (WL_{LC}/WL) within the main pipe. For the tested temperature ranges ($T_{LC}/T_U < 0.75$ and $T_{LC}/T_U > 1.25$), the detection limits for cold and warm connections are 0.025 and 0.015 respectively (Fig. 8), *i.e.* for every connection

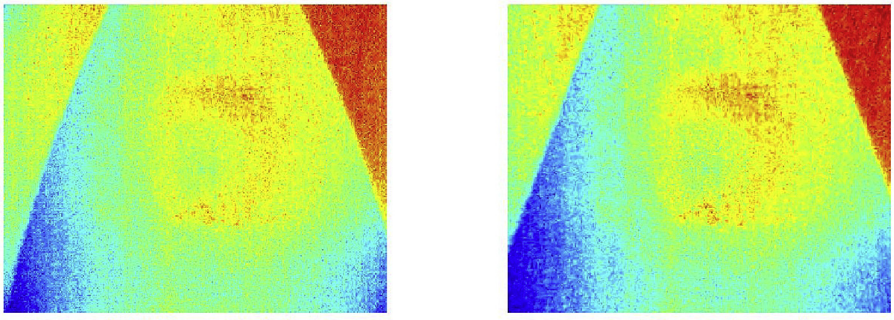

Fig. 4. Distortion correction for each frame: distorted (raw, left) and undistorted (corrected, right) images.

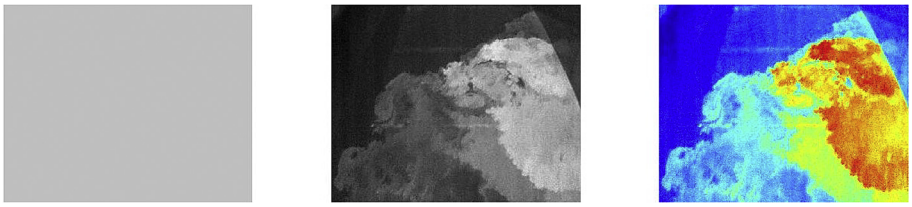

Fig. 5. Treatment of each frame: end-user friendly visualisation. From full scale on the left and after rescaling (middle) and the conversion to the blue-red scale. Discharge in the flume 100 l/s (15.9 °C) and a lateral discharge of 2.84 l/s (33.5 °C) coming through the connection D 200 mm (For interpretation of the references to colour in this figure legend, the reader is referred to the web version of this article.).

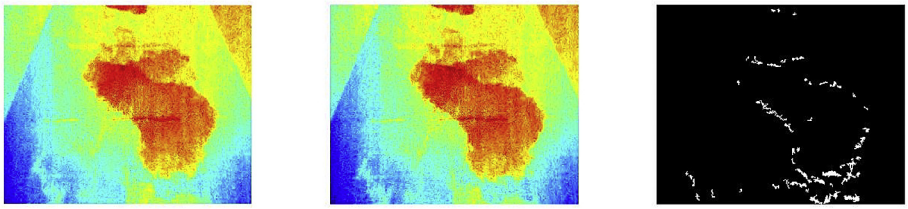

Fig. 6. Plots of two consecutive and undistorted frames on the left and in the middle, and the binary image of the difference after applying equation (4) on the right. Discharge in the flume 200 l/s (15.9 °C) and a lateral discharge of 2.47 l/s (27.5 °C) coming through the connection WL 400 mm.

and T_{LC} tested, all the connections offering a rate $Q_{LC,TRUE}/Q_U$ higher than 0.025 (for cold water) and 0.015 (for warm water) have been always detected by the proposed method (Fig. 7).

Fig. 9 (top part) depicts the influence of the ratio WL_{LC}/WL. For the smallest pipe diameter (WL 200 mm), 12 cold and 7 warm connections have not been detected. Pipes positioned higher show less non-detection results: 5 and respectively 2 cold connections have not been detected for the second (WL 400 mm) and respectively third pipe (WL 600 mm). Due to the different water density, warm connections are a bit more easily detectable than cold ones: this is an important drawback for rain water and groundwater infiltration detection in a sewer (except for runoff water during summer).

The cracks (simulated by the diffusor, Table 1) cannot be detected when they are completely submerged: the small discharge passing through them (*i.e.* low velocity at the outlet of the connection) or the linear geometry of the connection are the two likeliest reasons explaining this result.

While excluding experiments with the diffusors (485 remaining experiments), 347 connections have been detected: the detection ratio is equal to 0.72. Even at low turbulence levels ($Re = 37\,500$) the detection capabilities of the proposed method remain intact. However, Fig. 10 highlights the fact that the rate $Q_{LC,TRUE}/Q_U$ of non-detected connections is decreasing with increasing turbulence, especially for cold connections (blue circles): from 0.022 for a Reynolds of 37 500 to 0.0025 for a Reynolds 212 500.

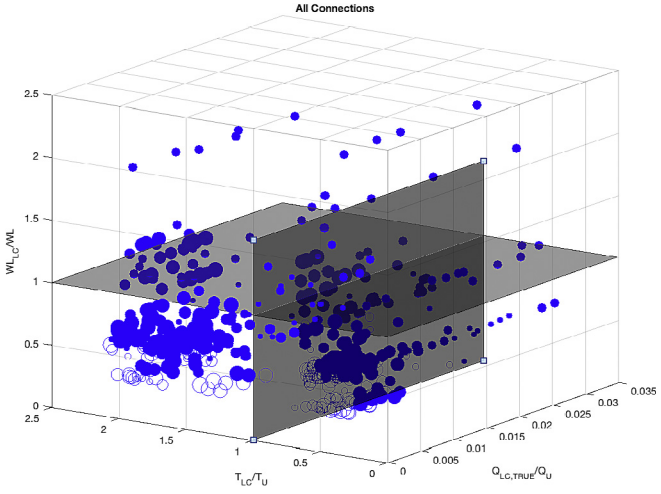

Fig. 7. 3D scatter plots of detection capability for all the connections. The filled markers are the detected connections. The T_{LC}/T_U and $Q_{LC,TRUE}/Q_U$ are the temperature and discharge ratios between the lateral connection and the flume respectively. The WL_{LC}/WL indicates the position of the lateral connection with respect to the water level. The bigger is the Marker size the higher is the Reynolds number (i.e. Q_U): 5 classes have been defined (100–120/200/300/400/500–520 l/s).

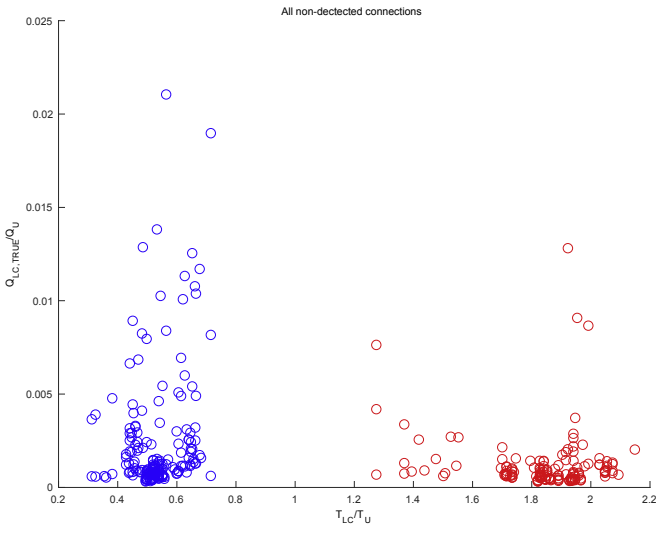

Fig. 8. 3D scatter plots of detection capability for the following connections: WL 200 mm (top-left), WL 400 mm (top right), I 100 mm (bottom left) and I 50 mm (bottom right). Same legend as in Fig. 7.

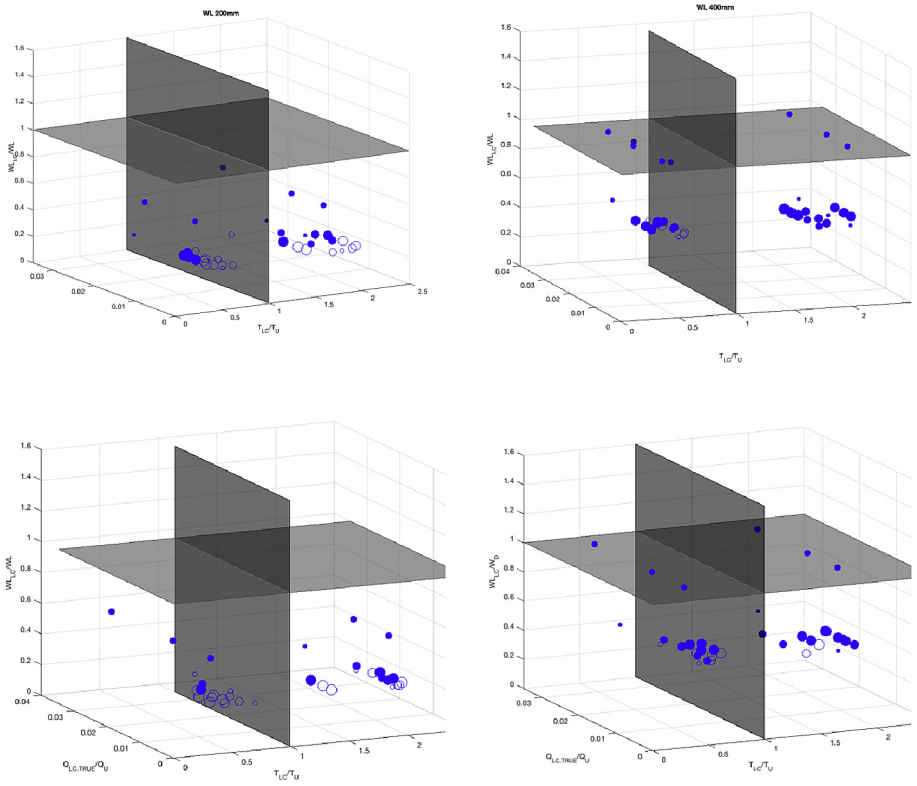

Fig. 9. 3D scatter plots of detection capability for the following connections: WL 200 mm (top-left), WL 400 mm (top right), I 100 mm (bottom left) and I 50 mm (bottom right). Same legend as in Fig. 7.

Intrusive connections are, surprisingly, more difficult to detect than non-intrusive ones. The detection ratio for the intrusive connections (I 50 mm, I 100 mm, I 150 mm, I 200 mm, M_D 75 mm and M_I 50 mm) is equal to 0.55. For non-intrusive connections, the detection ratio is equal to 0.85. This difference cannot be explained by the different diameter and relative elevation of the connection. Detection ratios are similar for both groups: 0.87 for D 200 mm (at 400 mm from the invert level), 0.81 for D 160 mm (at 400 mm from the invert level), 0.84 for all the WL and 0.86 for WL 400 mm. However, the number of non-detected connections are equivalent for WL 200 mm and I 100 mm (located at the same distance from the invert level). Comparison between WL 400 mm and I 50 mm leads to the same conclusion. The detection ratios are lower for long intrusions: 0.61 for I 150 mm and 0.48 for I 200 mm. Two main hypotheses can be expressed to explain those results. The first one is the contraction of the streamlines coming from the lateral connection due to the velocity distribution around the connected pipe. The second is derived from the secondary flow within a wet section (as illustrated in Bonakdari et al., 2008): if the discharge coming from the lateral connection is injected in the low velocity area of the wet section, inside the recirculation core, the warm (or cold) water might get confined within this recirculation zone. The lower detection rates found for the longer intrusion are in favour of the second hypothesis.

3.2.2. Quantification of the lateral discharge

For the quantification and the variance test (between the known discharge $Q_{LC,TRUE}$ and the estimated one $Q_{LC,IR}$), the following values of standard deviation have been used: $u(A_{TANK}) = 0.05$ m^2, $u(d) = 0.3$ s, $u(h_{BEGINNING}) = u(h_{END}) = 0.005$ m, $u(T_U) = u(T_D) = 0.01$ °C and $u(T_{LC}) = 0.05$ °C. These standard deviations on the water levels ($h_{BEGINNING}$ and h_{END}) are equal to the half-length of the smallest graduation (1 mm) of the used steel rule. The standard deviation of the tank area has been calculated by the law of propagation of uncertainty (JCGM 104, 2009), applied on the tank geometry (rectangular with four triangular shrink angles) and with a standard deviation of 1 mm for the measured distances (measured with a winding meter). The standard deviations of the temperatures at the flume free surface ($u(T_U)$ and $u(T_D)$) are evaluated from the resolution of the IR camera: 50 mK, *i.e.* 0.05 °C. The uncertainty of the temperature of the lateral connection comes from the same reasoning: it is derived from the resolution of the thermometer used for the measurement. Finally, the standard deviation of the duration (measured with a manual chronometer) comes from the widely admitted average human reflex to a visual stimulus: 0.3 s (Fondarai et al., 2009).

For every experiment where the lateral connection has been detected, the quantification (based on IR images) of the lateral connection discharge has been attempted.

In order to estimate T_U and T_D (Eq. (13)), a temperature map (Fig. 11) at the free surface has been composed for every retained experiment.

The location of the warm lateral connection is plotted by the black square and its effect is clearly visible of the map. However, Fig. 11 (bottom) illustrates the complexity of defining T_U and T_D, as there is no clear plateau in the average temperature. No clear plateau has been observed in all the experiments.

Despite this difficulty, the discharges coming from the lateral connections have been calculated while choosing arbitrary T_U (e.g. in Fig. 11: T_U = 18.8 °C, at ca. 12 m from the

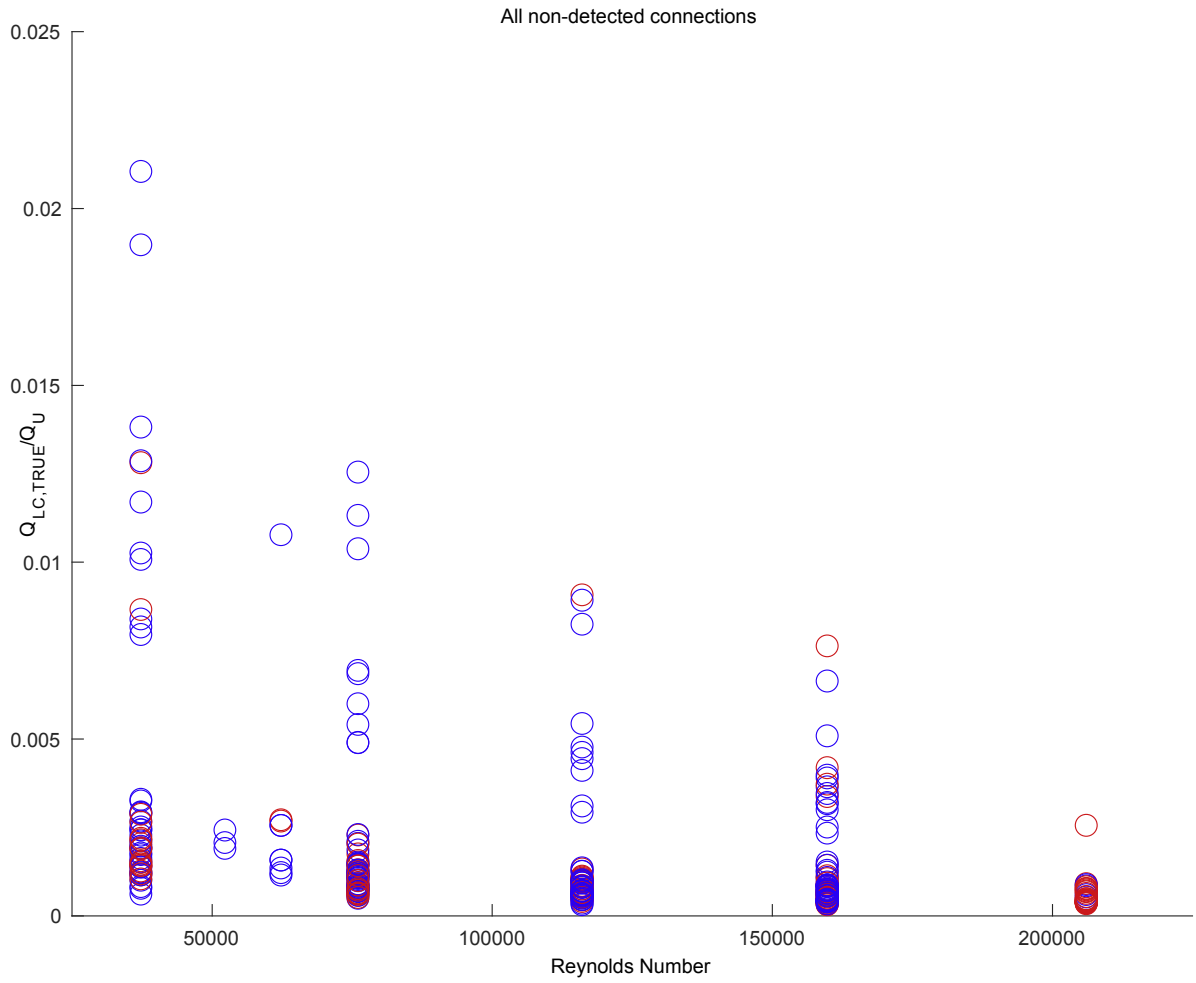

Fig. 10. Influence of the Reynolds number on the non-detection of lateral connections (warm: red, cold: blue). (For interpretation of the references to colour in this figure legend, the reader is referred to the web version of this article.).

downstream reference point). As illustrated by a first estimate (Eq. (7)) with the data from Fig. 11, the quantification has not been successful: $Q_{LC,IR}$ = 19.78 l/s instead of 2.84 l/s ($Q_{LC,TRUE}$). In every experiment, the difference between $Q_{LC,IR}$ and $Q_{LC,TRUE}$ are of the same order of magnitude (or one higher) than $Q_{LC,TRUE}$ (Fig. 12).

Among the exploitable 2D temperature maps (253 maps of the 347 detection), only 41 experiments gave some consistency between $Q_{LC,IR}$ and $Q_{LC,TRUE}$ (*i.e.* a consistency ratio of 0.16).

Despite the large residuals for the high discharges (Q_U of 500 and 520 l/s), the consistency ratio between $Q_{LC,IR}$ and $Q_{LC,TRUE}$ is relatively good (0.22). The consistency ratios increase with the discharge class: 0.12 for 100–120 l/s, 0.14 for 200 l/s, 0.23 for 300 l/s, 0.2 for 400 l/s and, as previously stated, 0.22 for 500 l/s. In fact, the higher Q_U is the bigger $u(Q_{LC,IR})$*is* (Eq. (11a) and Fig. 13).

Fig. 11 illustrates that the standard uncertainty of the lateral connection discharge ($u(Q_{LC,IR})$) is linearly dependant on the discharge in the main pipe (Q_U). For discharges greater than 400 l/s, $u(Q_{LC,IR})$ is greater than 10 l/s, *i.e.* at least of the same order of magnitude than the tested $Q_{LC,TRUE}$ (up to 3 l/s). Even assuming $u(Q_U) = 0.05 \times Q_U$ (more realistic assumption *in situ*), $u(Q_{LC,IR})$ will reach a value of 32 l/s (instead of 28 l/s) for Q_U = 1000 l/s. The proposed method is too uncertain for the main pipe having high discharges.

3.2.3. *Effect of inspection moving speed*

In order to test whether the moving speed of the train sensor has an impact on the produced results, a triplicate of similar experiments took place. All conditions were the same, apart for some small inevitable differences in the flows of the lateral connections, and the moving speed, which varied from low (~0.3 m/s) to fast (~1 m/s). The detection appears to be independent of the moving speed (Fig. 14), although the recorded cloud has a different shape. Despite the averaging algorithm, the fingerprint of the warm connection is still visible when the camera is moving at *circa* 1 m/s (bottom map). The thermal effects of the warm connection occur at the same location (ca 17 m from the reference point, *i.e.* ca *1.5* m of the active lateral connection). The lowest is the moving speed, the smoothest is the cloud of warm water at the free surface: more frames are used to build the average temperature at a specific location. Regarding the quantification of the lateral connection, this special experiment took place only once at a high flow in the flume (400 l/s), a parameter that leads to arbitrary results as previously discussed.

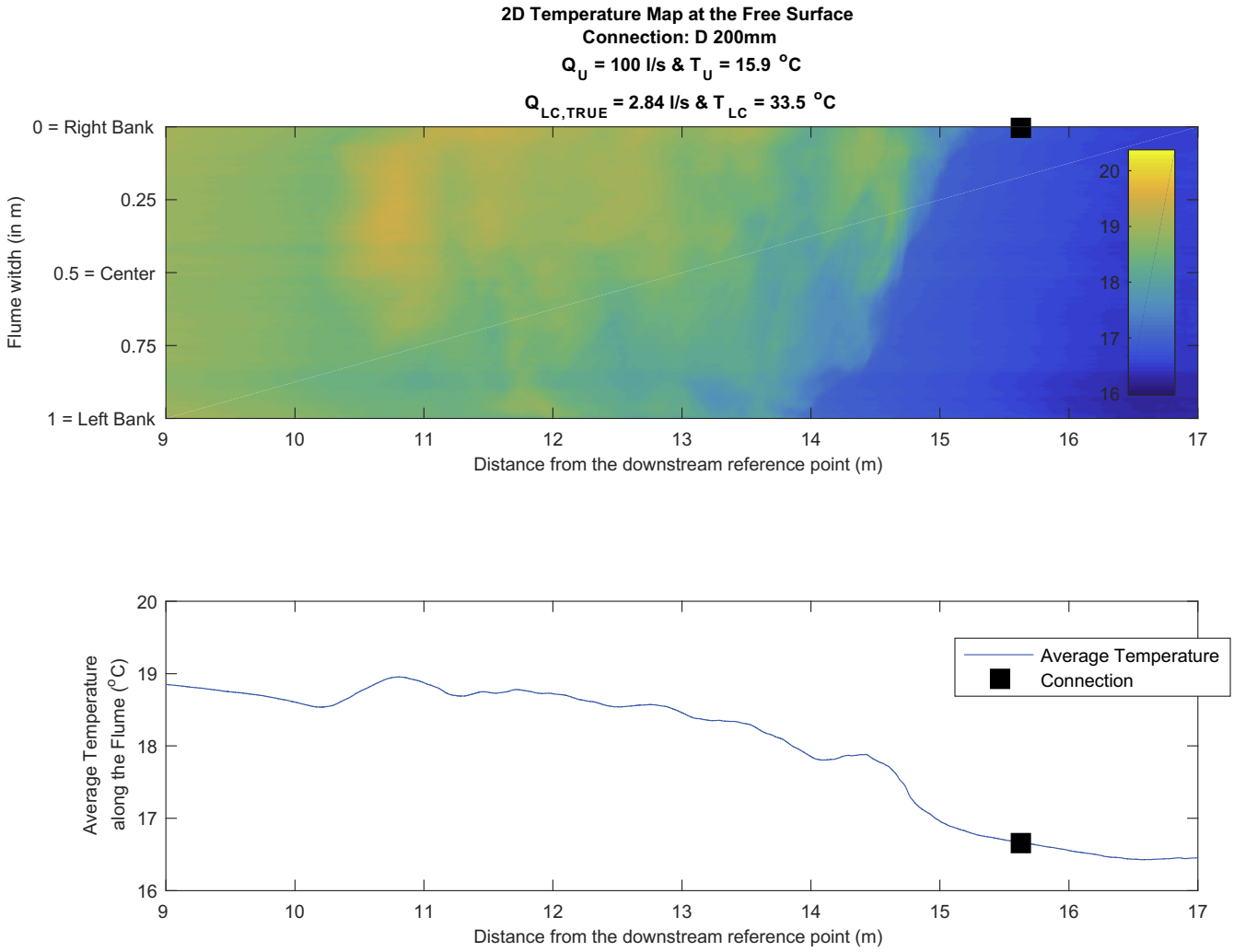

Fig. 11. A 2D temperature map of the free surface (top) with average temperature along the reach (bottom).

The detection is not affected by the moving speed up to 1 m/s. This conclusion allows for potential fast (and hence relative cheap) inspection within a sewer.

4. Conclusions and perspectives

The present study aims at proposing, testing and validating a new method to detect lateral connections on their thermal fingerprints. As the DTS, IR cameras appear to be powerful tools to detect those connections, especially since the measurement is done at the free surface (the most efficient location according to Nienhuis et al. (2013)). The data analysis of the 748 experiments demonstrate some serious pro's and con's of this technique in comparison to DTS.

The proposed method offers relatively low detection limits: below 2.5% for warm and 1.5% for cold water connections for the tested temperature ranges. Additional experiments are required to investigate a T_{LC}/T_U between 0.75 and 1.25. Unfortunately, those detection limits cannot be compared to the ones given by Nienhuis et al. (2013), expressed in terms of volume and not discharge. Furthermore, the *in situ* application of this method is relatively easy: a basic IR camera mounted on a floating device will allow for a fast inspection (moving speed up to 1 m/s). However, for such application, additional calculations will be needed to correct the position and orientation from the IR camera (e.g in Clemens et al., 2015). Furthermore, for the lateral connections close to the invert level (*i.e.* with a low WL_{LC}/WL), wrong non-detections may occur. Additional information are needed to locate such connection: *i)* sonar measurements for the interior pipe geometry to potentially detect the pipe of the connection (shape of the pipe or the connection itself, strange pattern in the sediment deposit due the lateral flow) and *ii)* accurate and refined velocity measurements to determine if the connection is active or not.

The quantification of lateral connections discharge seems to be unfeasible and too uncertain for pipes or reaches presenting high flows. The major drawback of the time method is its time-space dependency. By comparison, the installation of a DTS system in a sewer offers the capacity to measure in space (along the optical fiber) and over the time (e.g. few weeks). The lateral connection has to be active to be potentially detected by the moving IR camera: some luck or smart planning is required to apply efficiently this proposed method (e.g. infiltration and drainage connection

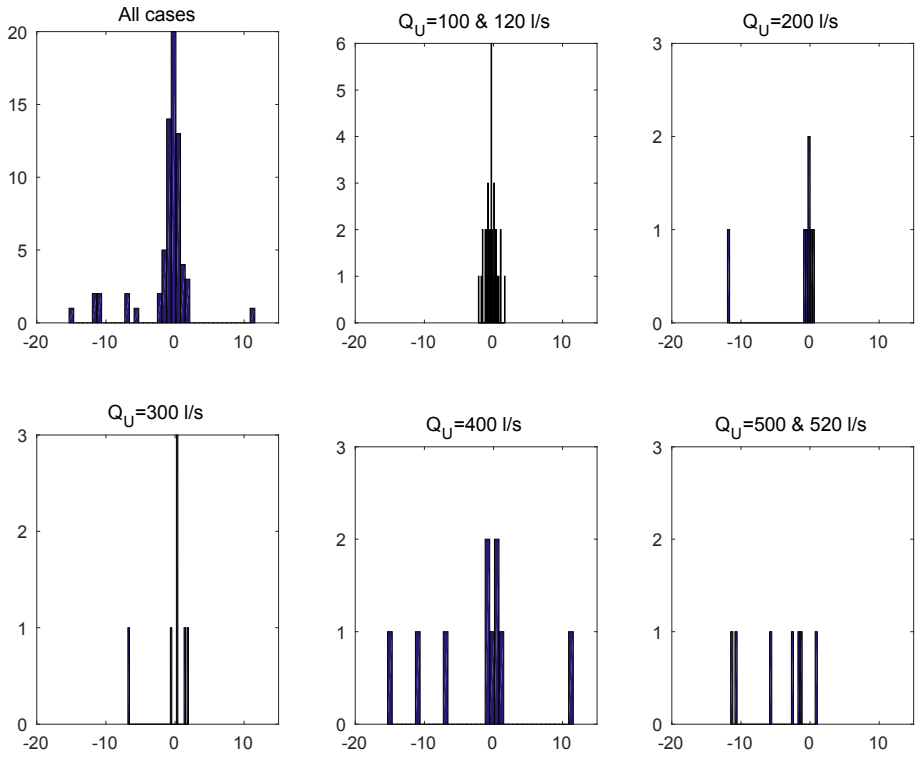

Fig. 12. Histograms of the residuals ($Q_{LC,IR} - Q_{LC,TRUE}$) in l/s, for the tested flows in the flume.

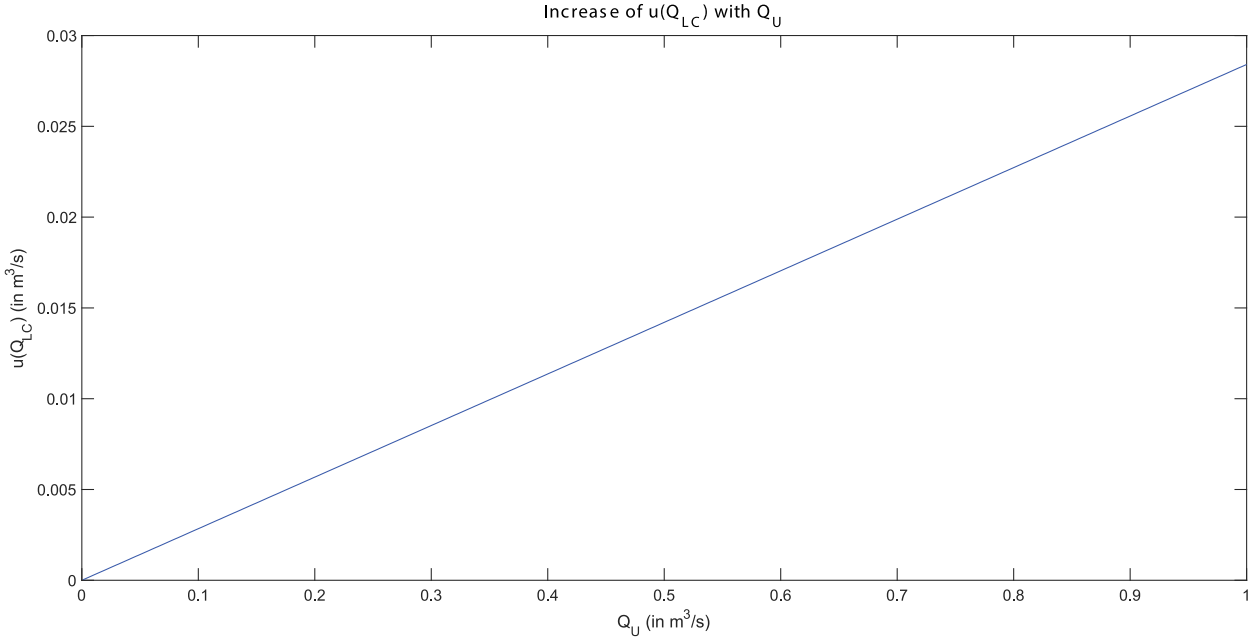

Fig. 13. Example of how the uncertainty $u(Q_{LC})$ evolves with respect to Q_U. Assumptions done for this plot: $T_U = 15$ °C, $T_{LC} = 20$ °C, $T_D = 16$ °C, $u(T_U) = u(T_{LC}) = u(T_D) = 0.05$ °C, $u(Q_U) = 0.01 \times Q_U$ and $cov(T_U, T_D) = u(T_U) \times u(T_D)$.

research during high water table periods or rain events). The detection of volunteer illicit connections might be more difficult: those connections might be voluntary disrupted during sewer inspections.

However, the present study highlighted the capacity of a basic IR camera for such an inspection. The proposed method appears to be more flexible than the installation of a DTS system. Future research will focus on field testing and integration of the described technique in a multi-sensor monitoring platform for sewer inspection.

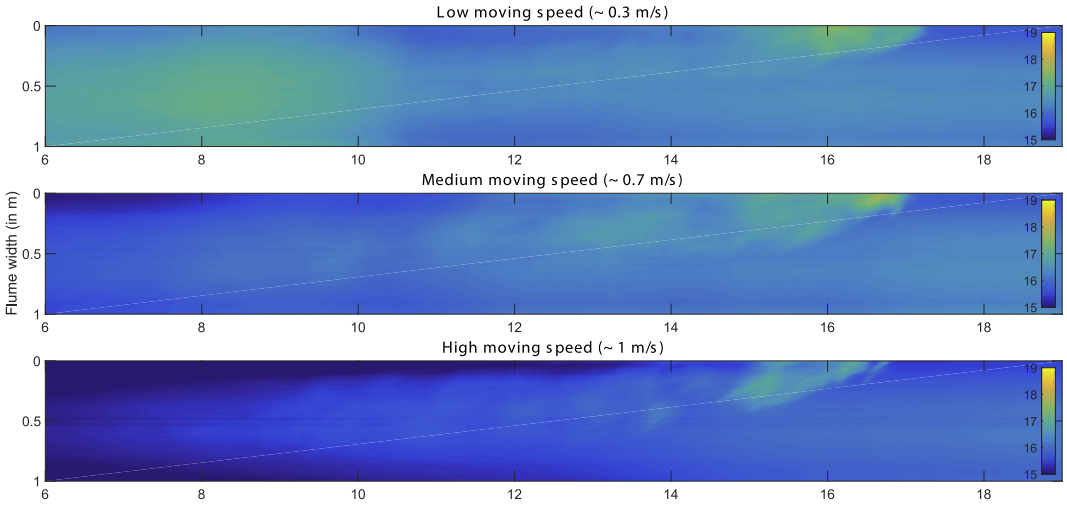

Fig. 14. Maps of similar experiments for different moving speeds of the sensor train. Discharge in the flume 400 l/s (15.8 °C). Tested connection: WL 600 mm. Top map (0.3 m/s): lateral discharge of 0.68 l/s (29.3 °C). Middle map (0.7 m/s): lateral discharge of 0.52 l/s (29.3 °C). Bottom map (1 m/s): lateral discharge of 0.58 l/s (29.3 °C).

Acknowledgements

Authors thank Foundation RIONED for funding this project, Deltares for making available their experimental facilities, Richard Boele and all technicians working with Deltares for their valuable support and interest in out work during the experimental work.

Appendix A

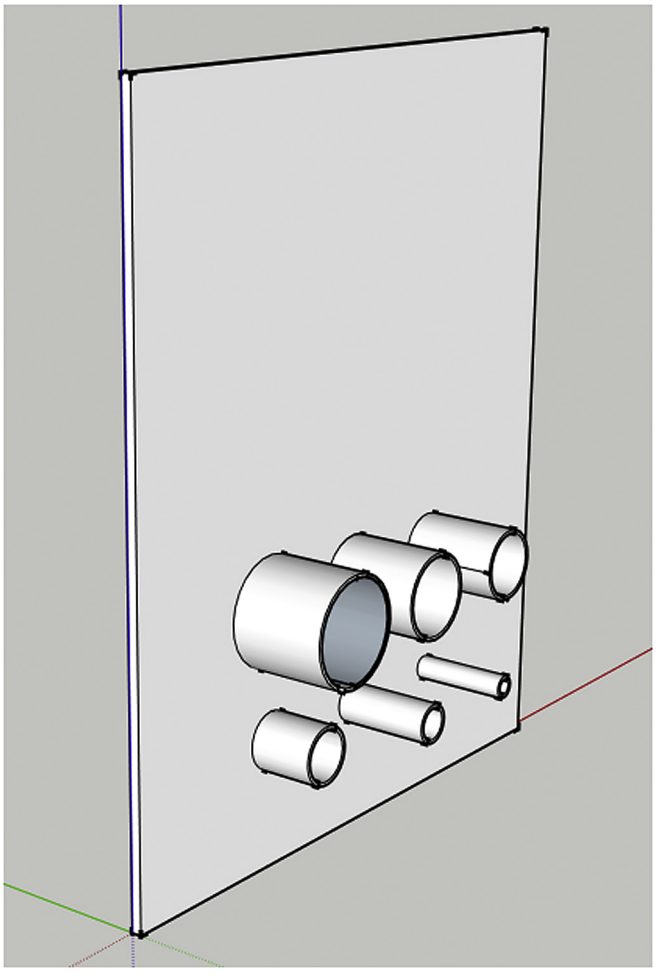

Fig. A1. Sketchup Make© screenshot of the Diameters window.

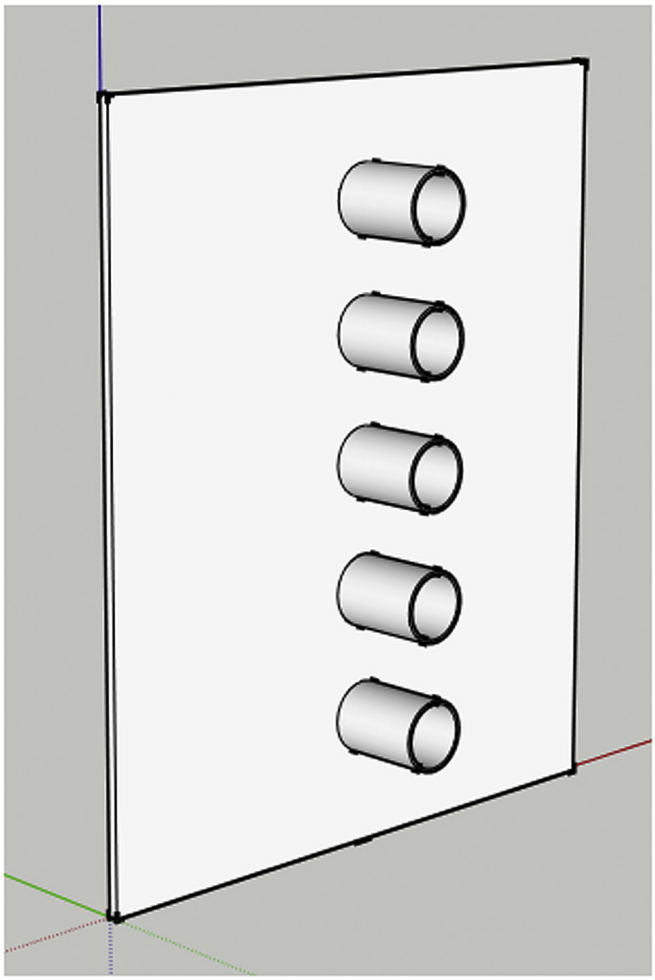

Fig. A2. Sketchup Make© screenshot of the Water Levels window.

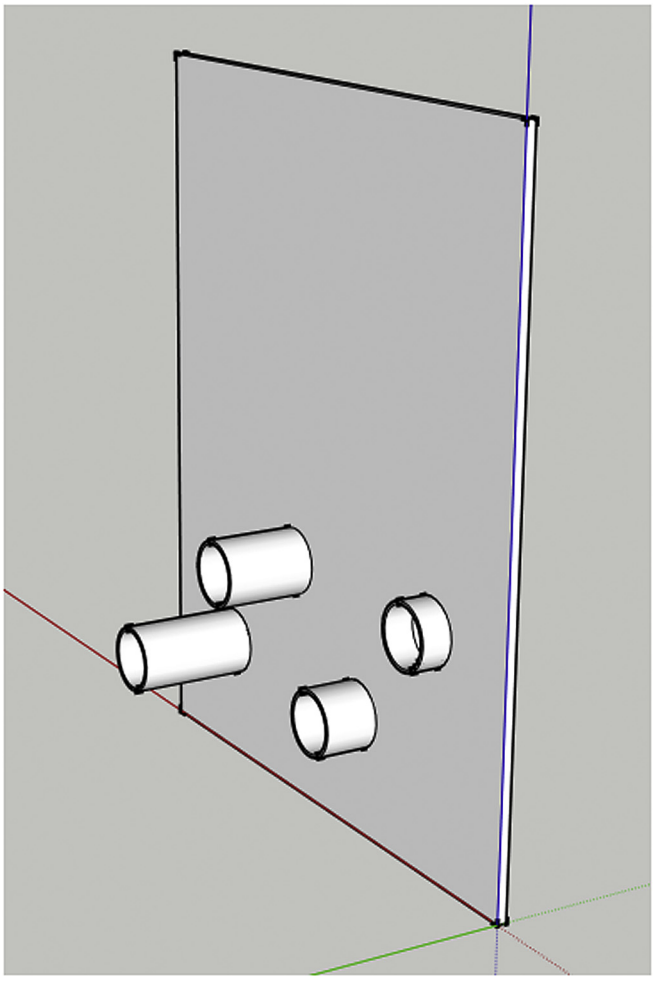

Fig. A3. Sketchup Make© screenshot of the Intrusions window (Side in the flume).

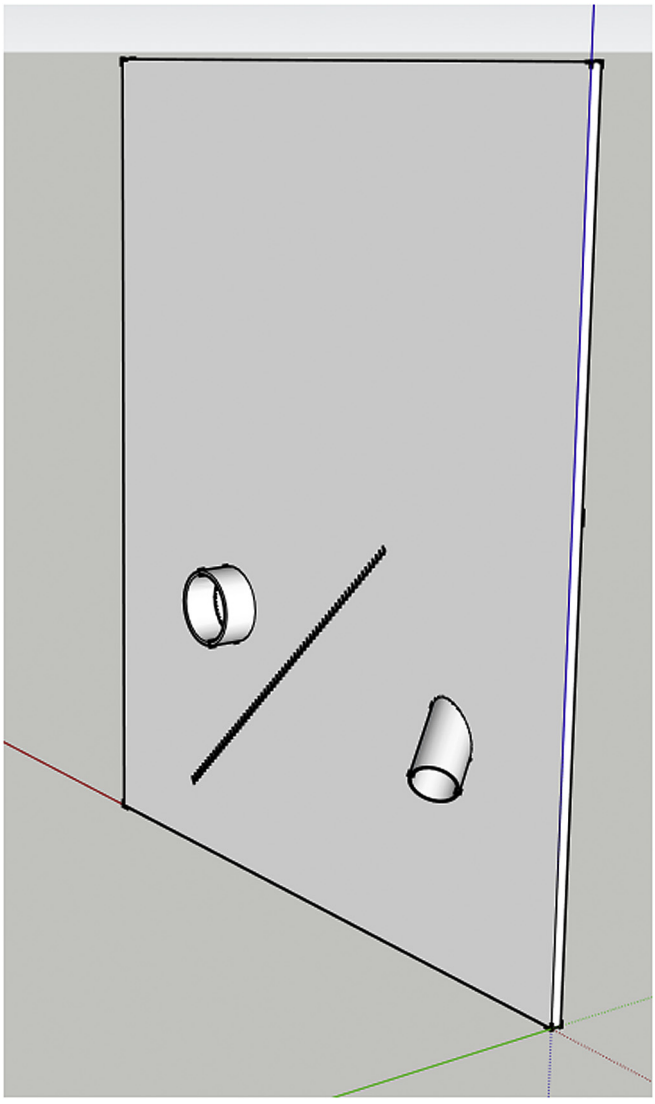

Fig. A4. Sketchup Make© screenshot of the Diameters window (Side in the flume).

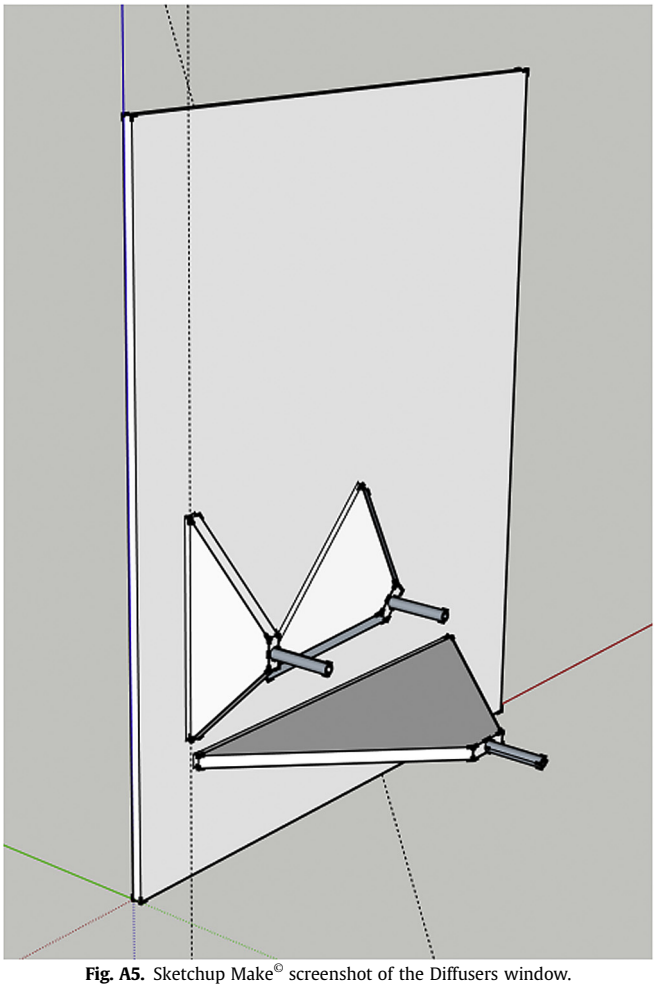

Fig. A5. Sketchup Make© screenshot of the Diffusers window.

References

de Bénédittis, J., Bertrand-Krajewski, J.-L., 2015. Mesurage de l'exfiltration en réseau d'assainissement par traçage au NaCl. La Houille Blanche 5, 26–34.

de Bénédittis, J., Bertrand-Krajewski, J.-L., 2005. Infiltration on sewer systems: comparison of measurement methods. Water Sci. Technol. 52 (3), 219–227.

Bertrand-Krajewski, J.-L., 2008. Programme Rw123etalo: 1st, 2nd and 3rd Order Polynomial Williamson Regression with Uncertainties in Both Variables for Sensor Calibration. INSA Lyon, LGCIE, Villeurbanne (France).

Bonakdari, H., Larrarte, F., Jonnais, C., 2008. Study of the shear stress in narrow channels: application to sewers. Urban Water J. 5 (1), 15–20. http://dx.doi.org/10.1080/15730620701726275.

Butler, D., Davies, J., 2004. Urban Drainage. CRC Press.

Clemens, François, Stanić, Nikola, Van der Schoot, Walter, Langeveld, Jeroen, Lepot, Mathieu, 2015. Uncertainties associated with laser profiling of concrete sewer pipes for the quantification of the interior geometry. Struct. Infrastruct. Eng. 11 (2015), 1218–1239. http://dx.doi.org/10.1080/15732479.2014.945466.

Deffontis, S., Breton, A., Vialle, C., Montréjaud-Vignoles, M., Vignoles, C., Sablayrolles, C., 2013. Impact of dry weather discharges on annual pollution from a separate storm sewer in Toulouse, France. Sci. Total Environ. 452–453, 394–403.

Fondarai, J.-A., Avril, P.-B., Michel, B.-F., Bartolin, R., 2009. Evolution of visual reaction time according to age: a meta-analysis of a total of 1 222 cases. Cah. l' Annee Gerontol. 1, 3–9.

Hoes, O.A.C., Schilperoort, R.P.S., Luxemburg, W.M.J., Clemens, F.H.L.R., van de Giessen, N.C., 2009. Locating illicit connections in storm water sewers using fiber-optic distributed temperature sensing. Water Res. 43 (20), 5187–5197.

JCGM 104, 2009. ISO/IEC Guide 98-Uncertainty of Measurement—Part 1: Introduction to Expression of Uncertainty in Measurement. ISO - International Organization for Standardization, Geneva (Switzerland).

Lega, M., Napoli, R.M.A., 2010. Aerial infrared thermography in the surface waters contamination monitoring. Desalination Water Treat. 23 (1–3), 141–151.

Nienhuis, J., de Haan, C., Langeveld, J., Klootwijk, M., Clemens, F.H.L.R., 2013. Assessment of detection limits of fiber-optic distributed temperature sensing for detection of illicit connections. Water Sci. Technol. 67 (12), 2712–2718.

Panasiuk, O., Hedström, A., Marsalek, J., Ashley, R.M., Viklander, M., 2015. Contamination of storm water by wastewater: a review of detection method. J. Environ. Manag. 152, 241–250.

Reed, B.C., 1989. Linear least-squares fits with errors in both coordinates. Am. J. Phys. 57 (7), 642–646.

Reed, B.C., 1992. Linear least-squares fitting with errors in both coordinates. II: comments on parameter variances. Am. J. Phys. 60 (1), 59–62.

Schilperoort, R.P.S., Gruber, G., Flamink, C.M.L., Clemens, F.H.L.R., van der Graaf, J.H.M.H., 2006. Temperature and conductivity as control parameters for pollution-based real-time control. Water Sci. Technol. 54 (11–12), 257–263.

Schilperoort, R., Hoppe, H., de Haan, C., Langeveld, J., 2013. Searching for storm water inflows in foul sewers using fibre-optic distributed temperature sensing. Water Sci. Technol. 68 (8), 1723–1730.

Williamson, J.H., 1968. Least-squares fitting of a straight line. Can. J. Phys. 46, 1845–1847.